Single-Cell Multiomics Analysis of Early Wound Response Programs in the Mouse Corneal Epithelium

Zhao-Jing Lu,[1,2] Jin-Guo Ye,[1] Jing-Ni Li,[1] Jiang-Bo Liang,[1] Ming Zhou,[1] Qiu-Ling Hu,[1] Qi-Kai Zhang,[1] Yu-Heng Lin,[1] and Ying-Feng Zheng[1,2]

[1]State Key Laboratory of Ophthalmology, Zhongshan Ophthalmic Center, Sun Yat-Sen University, Guangdong Provincial Key Laboratory of Ophthalmology and Visual Science, Guangzhou, China
[2]Research Unit of Ocular Development and Regeneration, Chinese Academy of Medical Sciences, Beijing, China

Correspondence: Ying-Feng Zheng, Zhongshan Ophthalmic Center, Sun Yat-Sen University, 7, Jinsui Road, Eye Center, Zhujiang New Town, Tianhe District, Guangzhou 510060, China;
zhyfeng@mail.sysu.edu.cn.
Zhao-Jing Lu, Zhongshan Ophthalmic Center, Sun Yat-Sen University, 7, Jinsui Road, Eye Center, Zhujiang New Town, Tianhe District, Guangzhou 510060, China;
luzhaojing@gzzoc.com.

ZJL and JGY contributed equally to this article.

Received: April 30, 2024
Accepted: February 11, 2025
Published: March 5, 2025

Citation: Lu ZJ, Ye JG, Li JN, et al. Single-cell multiomics analysis of early wound response programs in the mouse corneal epithelium. *Invest Ophthalmol Vis Sci.* 2025;66(3):9. https://doi.org/10.1167/iovs.66.3.9

Purpose. Wound healing is crucial for restoring homeostasis in living organisms. Although wound response mechanisms have been studied extensively, the gene regulatory programs involved remain to be elucidated. Here, we used single-cell RNA sequencing (RNA-seq) and ATAC sequencing (ATAC-seq) analysis to profile the regulatory landscape of mouse corneal epithelium in early wound response.

Methods. We used our previously published single-cell data sets of homeostatic adult mouse corneal epithelium as the unwounded group. The wounded group data sets were obtained by sequencing the epithelium after an annular epithelial wound. Following the integration of the relevant data sets, the Seurat and ArchR packages were employed for single-cell RNA-seq and single-cell ATAC-seq data processing and downstream analysis, respectively. The Monocle 2 was used for pseudo-time analysis, CellChat for intercellular communication analysis, and pySCENIC for analyzing transcription factors. The expression of key genes was validated via immunofluorescence staining and quantitative real-time PCR.

Results. Our data show that the number of cell type–specific genes decreases and the number of common transcriptional responses increases in early wound response. Concurrently, we find that the chromatin accessibility landscape undergoes significant changes across all epithelial cell types and that the wound-induced open regions are similarly distributed across the genome. Motif enrichment analysis shows that Fosl1/AP-1 binding site is highly enriched among the opened regions. However, by assessing the correlation between changes in chromatin accessibility and gene expression, we observe that only a small subset of wound-induced genes shows a high correlation with the accessibility of nearby chromatin.

Conclusions. Our study provides a detailed single-cell landscape for transcriptomic and epigenetic changes in mouse corneal epithelium during early wound response, which improved our understanding of the mechanisms of wound healing.

Keywords: corneal epithelium, wound healing, gene regulation program, single-cell analysis

Wound healing is an essential biological process that occurs following injury or infection, with the primary objective of restoring the normal homeostasis of living organisms.[1] Upon injury, the affected tissue promptly launches a series of highly ordered and coordinated responses, including inflammation, cell proliferation and migration, and tissue remodeling.[2] Deregulation of wound healing can lead to a chronic wound and even be life-threatening.[3,4] Therefore, understanding the molecular mechanisms of wound healing has long been an important focus in medicine and biology.

Epithelial tissue serves as a physical barrier against the external environment. Rapid and efficient wound healing after epithelial injury is critical for maintaining internal homeostasis. To date, using different models of epithelial injury, researchers have identified several important genes and signaling pathways essential for wound healing, such as jun N-terminal kinase (JNK) signaling, insulin and TOR signaling, and Hippo pathway.[5–10] Particularly in recent years, with the advancement of sequencing technologies, a more comprehensive understanding of this biological process has been achieved through genome-wide analysis. Many studies have shown that a large number of transcriptomic and epigenetic changes occur during tissue wound repair.[11–13] These wound-induced changes include both the repression of genes required for differentiation and the activation of genes required for motility, mainly involving regulating the expression of cell cycle regulators, matrix molecules, integrins, proteases, antioxidant enzymes, and so on. Despite these findings, the gene regulation programs involved in early response to epithelial wounds are still largely unknown, and the wound response

characterization of individual cells also remains to be elucidated.

Mouse cornea serves as an excellent model system for studying the mechanisms of wound healing.[14] Its epithelial layer comprises nonkeratinized stratified squamous cells, with each successive layer representing a more differentiated state. Following corneal epithelial injury, both limbal stem cells and central epithelial cells can mobilize toward the wound site and re-epithelialize the wound bed.[15–17] Similar to other stratified squamous epithelium, corneal epithelial wound healing can be divided into two phases.[18] The initial phase involves cellular and subcellular reorganization to trigger migration of the epithelial cells. Subsequently, the wound closure phase includes cell migration, proliferation, and differentiation. Therefore, findings derived from research in the corneal epithelium may be conserved and contribute to understanding the basic mechanisms of wound healing.

In the present study, we performed single-cell RNA sequencing and ATAC sequencing (scRNA-seq and scATAC-seq) analysis on epithelial cells from normal homeostasis (unwounded, UW) and wounded (WO) mouse cornea, and we characterized in detail the gene expression and chromatin accessibility changes during early wound healing. This may contribute to our understanding of wound healing and provide references for the development of treatment strategies of chronic epithelial wounds.

Methods

Animals and Corneal Epithelial Debridement Wounds

Equal numbers of female and male C57BL/6J mice (8- to 10-week-old) were used in this study. All animal experiments were approved by the Animal Use and Care Committee of Zhongshan Ophthalmic Center at the Sun Yat-Sen University, in accordance with the ARVO Statement for the Use of Animals in Ophthalmic and Vision Research. Corneal epithelial debridement was performed as previously described with minor modifications.[19] Mice were weighed and anesthetized by intraperitoneal injection of sodium pentobarbital (50 mg/kg), and ocular surface anesthesia was induced using 0.5% proparacaine. The corneal epithelium was then removed using an ophthalmic rotary burr (Algerbrush II, Alger Company Inc., Lago Vista, TX, USA) between two regions delineated by 2-mm and 3-mm trephines. After wounding, sterile saline was applied to remove cell debris, and tobramycin eye ointment was applied to prevent bacterial infection.

Single-Cell Isolation

Eyes were enucleated at 3 hours (recovery time for mice after anesthesia was approximately 1 hour), and cornea dissociation and single-cell isolation were performed as previously described, with modifications.[20,21] Briefly, the dissected cornea tissues were pooled and incubated with 0.25% trypsin for 30 to 50 minutes at 37°C. The loose central corneal epithelial sheets were peeled and digested with fresh trypsin. Then cells were collected into RPMI medium containing 10% fetal bovine serum to deactivate and remove trypsin. Cell suspension was centrifuged, resuspended, and filtered using a cell strainer to ensure single-cell suspension. In this study, we pooled cornea epithelium from five male and five female mice into one sample, and a total of three samples were prepared.

Single-Cell Library Generation, Data Processing, and Quality Control

Single-cell RNA and ATAC library generation were performed following the 10× Genomics instructions (10× Genomics, Pleasanton, CA, USA), as previously described.[22] The FASTQ files were aligned using 10× Genomics Cell Ranger. Each library was aligned to the GRCm38.p3 mouse reference genome and quantified using the Cell Ranger (v3.1.0) count function.

Quality control parameters for scRNA-seq were used to filter cells with fewer than 1000 or more than 4200 genes, or a mitochondrial gene ratio greater than 5%. The batch effect across different samples was removed using the Harmony package.[23,24]

Quality control parameters for scATAC-seq were used to filter cells with fewer than 3200 unique fragments and enriched at transcription start sites (TSSs) below 5. Additionally, cells that mapped to blacklist regions based on the ENCODE project reference were removed.

Dimensionality Reduction and Clustering

For scRNA-seq data, dimensionality reduction was performed using the principal component analysis (first 10 principal components), and cell clusters were visualized with the uniform manifold approximation and projection (UMAP) algorithm. For scATAC-seq data, we performed a layered dimensionality reduction approach using latent semantic indexing and singular value decomposition, followed by Harmony batch correction based on each sample. Single-cell accessibility profiles were clustered using Seurat's shared nearest-neighbor graph clustering with "FindClusters" at the default resolution of 0.8 on the harmonized latent semantic indexing (LSI) dimensions.[23] All data were visualized using UMAP in a two-dimensional space.

Signature Score Analysis

Gene scores were calculated as follows: the score of the gene set in the given cell subset (referred to as X) was computed as the sum of all unique molecular indentifier (UMI) for all the genes expressed in X cells, divided by the sum of all UMI expressed by X cells.[25] The gene sets, obtained from published literature, are listed in Supplementary Table S1.[26]

scRNA-Seq Pseudo-Time Trajectory Analysis

Pseudo-time analysis of corneal epithelial cells was performed using Monocle 2 (v2.30.1) with default parameters.[27] Differentially expressed genes were identified by finding genes that change as a function of pseudo-time. The architecture of the pseudo-time trajectory was plotted using the DDRTree dimensionality reduction algorithm.

Cell–Cell Interaction Analysis

CellChat (v1.6.1) was used to analyze cell–cell interactions with default parameters.[28] Ligand–receptor interactions were analyzed using single-cell transcriptomic data across different corneal epithelial cell types.

Investigative Ophthalmology & Visual Science

Gene Activity Scores

Gene activity scores were calculated based on the accessibility within the gene body, at the promoter, and at distal regulatory elements. These scores were then correlated with gene expression using ArchR v1.0.2 with default parameters.[29] We applied the MAGIC imputation method to the resulting gene activity scores, aiming to reduce the noise associated with the sparsity of the scATAC-seq.[30]

Motif Enrichment and Motif Deviation Analysis

We performed motif enrichment and deviation analyses for the differentially accessible regions (DARs) using the "findMotifsGenome.pl" function in HOMER and the "addMotifAnnotations" function in ArchR.[31] Additionally, we computed chromCAR deviation scores for these motifs using the ArchR implementation.

Transcription Factors Footprint Analysis

We performed motif footprint analysis by measuring Tn5 insertions in genome-wide motifs and then normalizing these by subtracting the impact of Tn5 bias from the footprint signal. For each identified peak set, the "getPositions" function was utilized to calculate the positions of the motifs. These footprints were further normalized using the mean values ±200 to 250 bp from the motif center.

Transcription Factor Prediction

To identify transcription factors in corneal epithelial cells from our scRNA-seq data, we conducted single-cell regulatory network inference and clustering in Python (v3.12.2) with pySCENIC package (v0.12.1).[32] We extracted the count matrix from the Seurat object, converted it into CSV format, and then converted the CSV file to a loom format file as the input of pySCENIC. Next, a three-step process of pySCENIC was carried out. First, the GRNboost2 was used to infer the gene–gene coexpression relationships between transcription factors and candidate targets. Second, the regulon prediction was performed. Each regulon contained one transcription factor (TF), and its target genes enriched for the motifs of the TF. Finally, the activity scores of each regulon in each cell were evaluated using the AUCell algorithm. The pySCENIC output in the form of a loom file was subsequently analyzed utilizing the SCopeLoomR R package (V0.13.0). To identify cell condition–specific TFs, we used the regulon specificity score (RSS) method implemented in the calcRSS function in the R package SCENIC (v1.3.1). The analysis results were visualized with pheatmap R package (v1.0.12).

Integration of scRNA-Seq and scATAC-Seq Data

By directly aligning cells from scATAC-seq with cells from scRNA-seq, the union of the 2000 most variable genes was used in each modality as input to Seurat's "FindTransferAnchors" function and Seurat's "TransferData" function with "Weight reduction" set to the dimensionality of the scATAC-seq data set after Harmony batch correction. Other parameters were set to default. For each cell profiled by scRNA-seq and each cell profiled by scATAC-seq, we identified the nearest-neighbor cell in the respective other modality by applying a nearest-neighbor search in the joint CCA L2 space. These nearest-neighbor-based cell matches from all gestational time points were concatenated to obtain data set–wide cell matches across both modalities.

Peak-to-Gene Linkage Analysis

For the peak-to-gene linkage analysis, we employed the "addPeak2GeneLinks" function to compute peak accessibility and gene expression, setting the parameters "corCutOff = 0.2" and "reducedDims" as the results of dimensionality reduction after batch correction. The resultant "Granges" object was subsequently used for visualization.

Gene Ontology Analysis

The Gene Ontology (GO) analysis was conducted using the Metascape webtool (www.metascape.org). *P* values of GO terms and gene ratio were calculated based on the accumulative hypergeometric distribution by the Metascape webtool.[33]

Immunofluorescence Staining

For immunofluorescence staining, mouse corneal cryosections were fixed with 4% paraformaldehyde for 30 minutes at room temperature (RT) and then rinsed with PDT (PBS solution containing 1% DMSO and 0.1% Triton X-100) for 10 minutes and blocked with blocking solution (PDT containing 1% BSA and 10% normal goat serum) for 1 hour at RT. Primary antibodies were prepared in blocking solution containing 2% normal goat serum, and slides were incubated overnight at 4°C. Slides were washed three times with PDT and incubated with Alexa Fluor 488 nm secondary antibody for 1 hour at 37°C. DAPI was used to label the nucleus. The slides were washed three times with PBS and then mounted under glass coverslips. Finally, the fluorescence images were captured using a confocal laser-scanning microscope (Zeiss LSM 980; Zeiss, Oberkochen, Germany). The antibodies are listed in Supplementary information Table 1.

RNA Extraction and Quantitative RT-PCR

Total RNA of mouse cornea was extracted using Trizol (Takara, Kusatsu, Japan) and quantitated by NanoDrop spectrometry. cDNA was generated with the HiScript II Q RT SuperMix QPCR kit (Vazyme, R223-01, Nanjing, China). The mRNA levels were analyzed using ChamQ SYBR Color QPCR Master Mix (Vazyme, Q411-02). Gene primers are listed in Supplementary information Table 2.

Data and Code Availability

The scRNA-seq and scATAC-seq data of mouse corneal epithelial cells under normal homeostasis were obtained from our previous study (GRA009182). The raw sequence data associated with corneal wounding reported in this study are available at the Gene Expression Omnibus with accession number GSE285349. Sample metadata are presented in Supplementary Table S2.

The data analysis pipeline in our study was performed according to the description on the 10× Genomics website (https://www.10xgenomics.com), Seurat website (https://github.com/satijalab/seurat), and ArchR website (https://www.archrproject.com). The associated reference code is available via GitHub (https://github.com/RyanYip-Kat/yipCat; https://github.com/RyanYip-Kat/find2Kat).

Results

Single-Cell Multiomics Analysis of the Mouse Corneal Epithelium

In this research, we used our previously published single-cell sequencing data sets of homeostatic adult mouse corneal epithelial cells, from which central cornea basal cells, corneal wing cells, and corneal superficial cells were extracted as the unwounded control group.[34] The wounded group data sets were obtained by performing 10× Genomics scRNA-seq and scATAC-seq on mouse corneal epithelial cells at 3 hours after an annular wound, a time point corresponding to the early stage of wound healing, before re-epithelialization (Fig. 1A; Supplementary Fig. S1).[15] After quality controls and sample integration using the Harmony algorithm, a total of 30,912 (9428 from two UW biological replicates; 21,484 from three WO biological replicates) cells from scRNA-seq and 43,939 (13,248 from two UW biological replicates; 30,691 from three WO biological replicates) cells from scATAC-seq were retained for the following analysis (Supplementary Figs. S2A–I).

With our scRNA-seq data, we identified the major cell types of the corneal epithelium, visualized in two-dimensional space using UMAP (Figs. 1B, 1E). Corneal basal cells (CBs) were annotated according to the previously reported marker genes *Itgb4* and *Gja1*.[35,36] Corneal wing cells (CWs) were identified based on the high expression

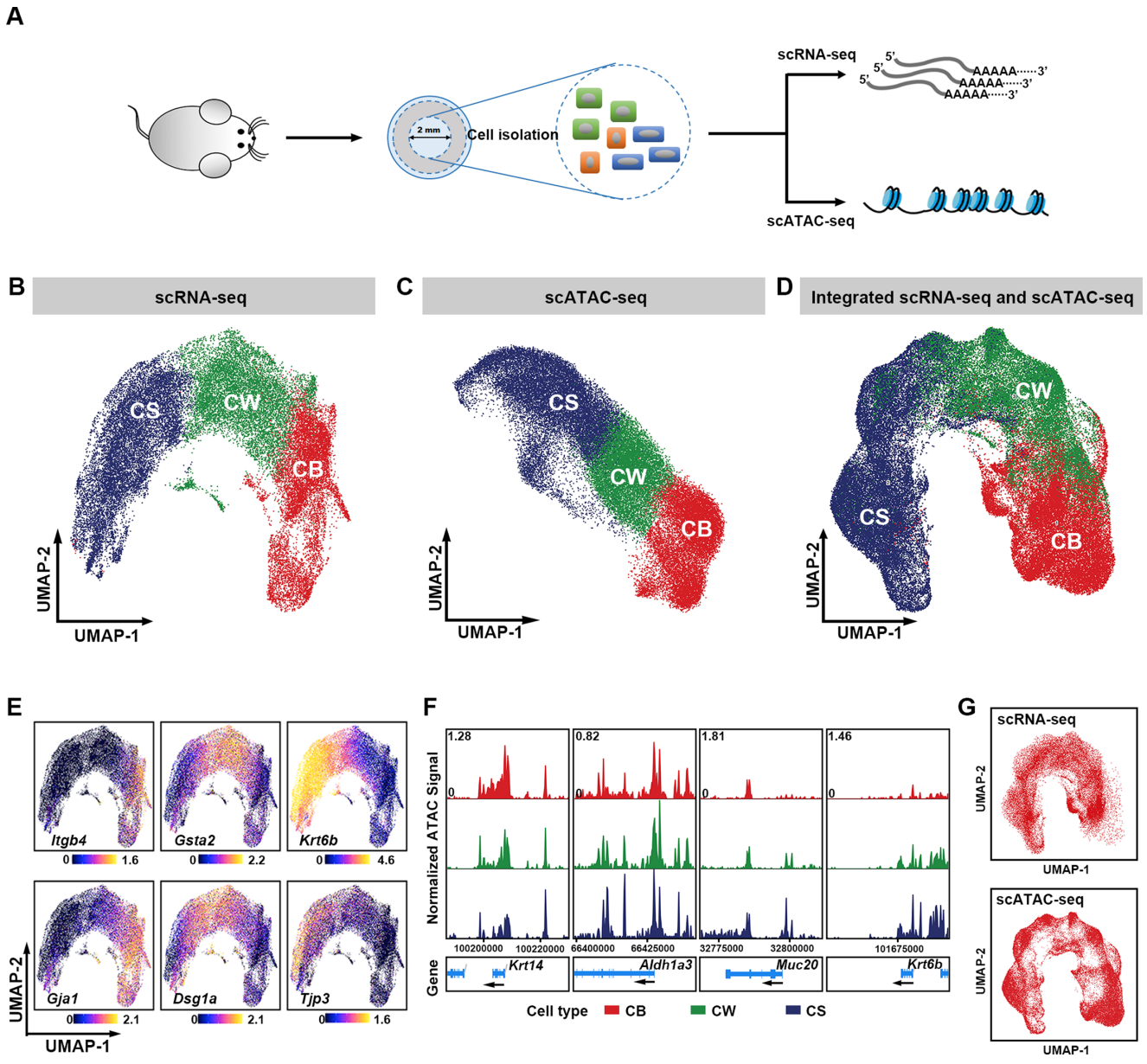

Figure 1. Single-cell chromatin accessibility and transcriptome profiling of epithelial cells in the UW and WO mouse corneas. (**A**) Schematic of experimental design for the single-cell analyses. (**B**, **C**) UMAP visualizations of the scRNA-seq (**B**) and scATAC-seq (**C**) data set. Each dot represents a single cell colored by its corresponding cell type. (**D**) UMAP visualization of the pooled scATAC-seq and scRNA-seq data sets; cells are colored by cell type. (**E**) Feature plots showing expression of the marker genes in the corneal epithelium. Normalized expression levels for each cell are color-coded and overlaid onto the UMAP plot. (**F**) Genome browser tracks showing single-cell chromatin accessibility in the marker gene locus. Each track displays pseudo-bulk ATAC data aggregated and colored by cell type. (**G**) Integrated UMAP as in (**D**).

of *Gsta2* and *Dsg1a*.[34] Cells expressed higher levels of *Tjp3* and *Krt6b*, representing the terminally differentiated corneal superficial cells (CSs).[34]

Likewise, we identified the same cell types using our scATAC-seq data (Figs. 1C, 1F). Cluster-based pseudo-bulk ATAC-seq signal showed higher chromatin accessibility at gene bodies of *Muc20* and *Krt6b* in CSs, indicating that they were terminally differentiated cells. CWs and CSs exhibited higher chromatin accessibility at the gene body of *Alhd1a3*, which is consistent with our previously reported localization of this protein in the corneal epithelium.[34] We noticed that there were also more open chromatin regions on the *Krt14* gene in CWs, suggesting that its expression was elevated after injury, which is consistent with a previous study reporting that its gene expression increased significantly 24 hours after injury.[37] Moreover, we performed gene activity score analysis with marker genes (*Itgb4*, *Col17a1*, *Dsc2*, *Cldn4*, *Krt6b*, and *Tjp3*) and further clarified the cellular identities (Supplementary Fig. S3A).

Finally, we integrated our scRNA-seq and scATAC-seq data sets according to the integration pipeline described in ArchR and Seurat. Cell types classified using transcriptome data and chromatin data were grouped together in the integrated UMAP space (Figs. 1D, 1G). Cell identities were confirmed by gene activity and gene expression in a panel of cell-type marker genes (Supplementary Fig. S3B).

Collectively, these data provide a general overview of the major cell types of the corneal epithelium during homeostasis and wound-healing state, indicating no dramatic changes in cell types in the early stage of wound healing.

Identification of Transcriptomic Changes in Early Wound Response

To characterize wound-induced transcriptomic changes in different cell types, we first compared the differentially expressed genes (DEGs) of each cell type under UW and WO conditions and subsequently analyzed the overlap of these DEGs across different cell types (Supplementary Figs. S4A–C; Fig. 2A). Upset plot analysis showed that the three cell types shared a large number of wound-induced upregulated genes, indicating that different corneal epithelial cells had similar patterns of gene expression in the early stages of wound healing (Fig. 2A; Supplementary Table S3). Among these shared genes, *Hif1a*, *Atf4*, and *Mdm2* have been identified and validated to be upregulated in many previous stress response–related studies[38–40] (Figs. 2A, 2B; Supplementary Fig. S4D). This demonstrated that our single-cell data were sensitive to identifying transcriptomic changes during early wound response.

GO analysis of the cell type–shared and cell type–specific DEGs after wounding indicated that genes related to regulation of the apoptotic signaling pathway and chromatin remodeling were greatly upregulated in all cell types, while genes associated with cell fate commitment were significantly decreased in all cell types (Figs. 2C, D). In addition, we found that genes involved in the PI3K-AKT pathway, epithelial-mesenchymal transition (EMT), wound healing, and corneal keratinization, among others, were also upregulated in the three cell types, which are important signaling pathways for wound healing (Fig. 2E; Supplementary Fig. S5). As expected, both UW and WO cornea epithelium did not express cornification-related genes.

Further, we validated some DEGs by performing immunofluorescence (IF) staining on mouse corneal tissue cryosections (Fig. 3A). In UW corneas, Krt14 is mainly located in the basal layer of epithelial cells, and Pax6 is expressed throughout the entire corneal epithelium. However, in WO corneas, we found that Krt14 was also highly expressed in the CW and CS layers, and Pax6 expression was significantly decreased in all cell types. Results from quantitative real-time PCR showed that *Krt14* expression was significantly elevated and *Pax6* expression was significantly decreased (Fig. 3B). These results are consistent with our transcriptomic data, indicating increased mobility and reduced differentiation of corneal epithelium during early wound healing. Meanwhile, we also found that Dsc2, a component of intercellular desmosome junctions, showed disrupted localization in wounded corneal epithelium, implying reduced cell adhesion.

Pseudo-Time Trajectory Analysis of Cell State Transition Dynamics

Then, we applied Monocle 2 to analyze the wound-induced changes in the context of corneal epithelial differentiation. In both UW and WO corneas, we observed a continuous trajectory of cell differentiation extending from the CB cell type to the CS cell type (Figs. 4A–D). A total of 11,416 and 10,010 pseudo-time-dependent genes were identified from the UW and WO data sets, respectively, of which 9247 genes overlapped (Fig. 4E; Supplementary Table S4). We found that the expression patterns of most overlapping genes along the pseudo-time trajectory were similar in UW and WO, with overall reduced expression levels (Fig. 4F).

Meanwhile, we compared the DEGs between different cell types in UW and WO corneas, respectively (Supplementary Fig. S6A). We used the known cell-type markers to determine cell identity (Supplementary Fig. S6B). The number of cell type–specific DEGs in WO was significantly reduced, but these specific genes still overlapped highly with those in UW (Supplementary Fig. S6C). We found that some marker genes, such as *Itgb1*, *Itgb4*, *Muc20*, and *Tjp3*, were downregulated in WO corneas (Supplementary Fig. S6D). Combined with the results of pseudo-time analysis, our data suggest loss of corneal epithelial cell identity during early wound response. Remarkably, a transient loss of transcriptional identity was also reported during the early stages of dorsal root ganglion neuron injury.[41] The mechanism and physiologic significance of this phenomenon in different tissues may warrant further exploration.

Interactions Between Corneal Epithelial Cells During Early Wound Healing

Based on the expression of the ligand–receptor gene in single cells, we also compared changes in cellular interactions between different epithelial cell types in the UW and WO corneas. Our data illustrate potential cross-talk between different epithelial cell types, but the number and weights/strength of the inferred interactions decreased in the wounded corneas compared to the unwounded corneas (Figs. 5A, 5B; Supplementary Figs. S7A, S7B). We observed signaling pathways related to cellular adhesion, proliferation, and growth, such as DESMOSOME, FN1, EGF, and WNT, were exclusively or more active in the UW cornea (Figs. 5C–E; Supplementary Fig. S7C). Among these path-

Investigative Ophthalmology & Visual Science

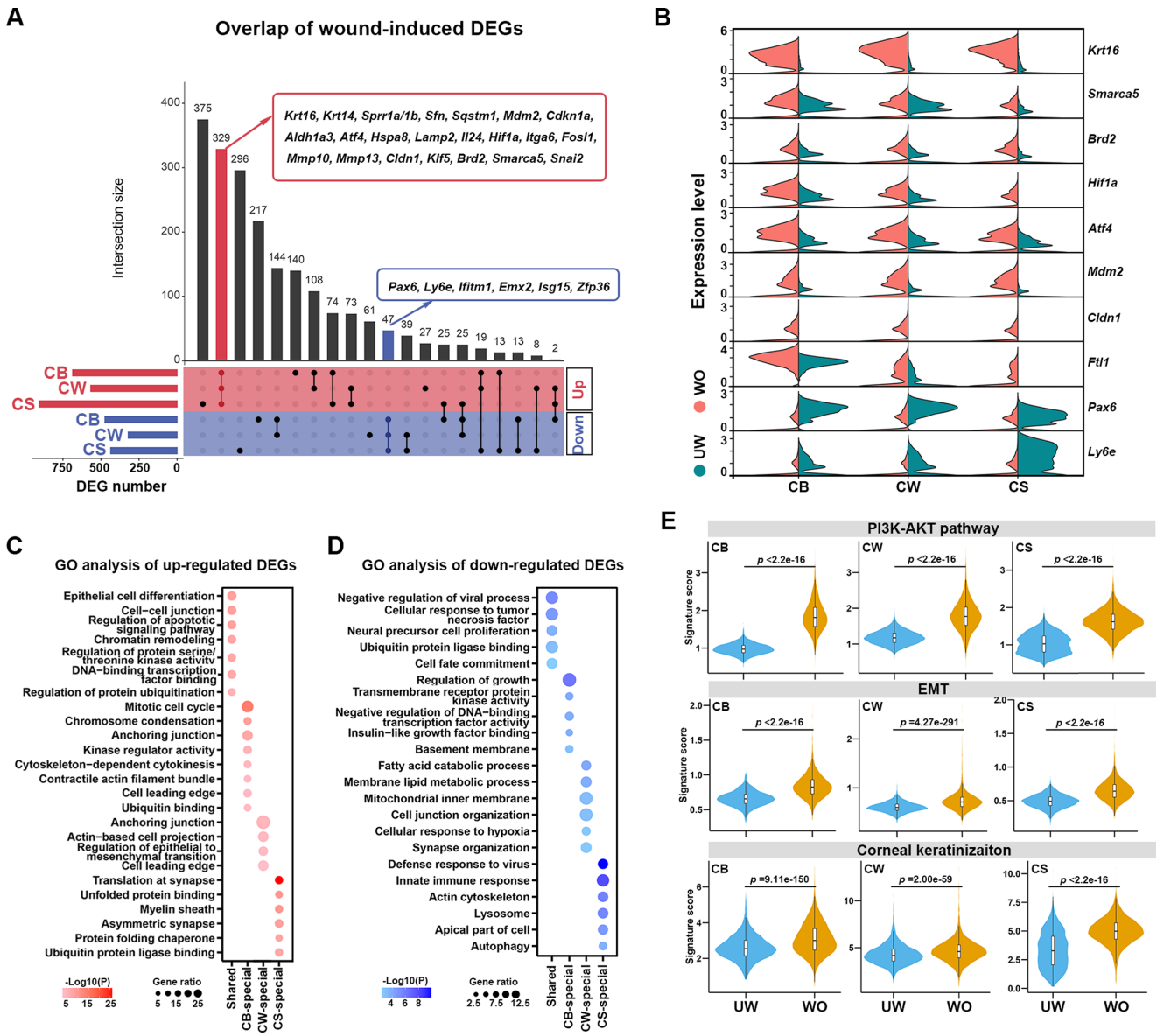

Figure 2. Early wound-induced gene expression changes in the corneal epithelium. (**A**) Upset plot showing the size of overlaps between the sets of wound-induced upregulated and downregulated DEGs identified in each cell type. The *bar graph* on the *left* shows the set size of upregulated and downregulated DEGs for each cell type, and the *bar graph* at the *top* shows the number of overlapping genes between different sets or the number of unique genes in one set. (**B**) Violin plots of select gene expression in each cell type, split by UW and WO samples. (**C**, **D**) GO term enrichment of early wound-induced upregulated (**C**) and downregulated (**D**) different expression genes. (**E**) Gene scoring analysis using the indicated molecular signatures. *P* values are from two-sided Wilcoxon rank-sum tests.

ways, the Notch signaling pathway is known to have an important role in corneal epithelial homeostasis maintenance and wound repair. Our results showed that Notch signaling was reduced in the WO compared to the UW, which is consistent with previous reports that a decrease in Notch1 expression promotes corneal epithelial cell migration during the early stages of wound healing[42,43] (Figs. 5F–I; Supplementary Fig. S7D).

Characterization of Chromatin Accessibility Changes in Early Wound Response

Then, we analyzed wound-induced DARs in different cell types of corneal epithelium. By comparing chromatin accessibility changes between UW and WO, we identified that 16,020, 16,897, and 15,161 peaks in WO were more accessible in CBs, CWs, and CSs, respectively, while 7625, 9073, and 8703 peaks in UW were more accessible in CBs, CWs, and CSs, respectively (Fig. 6A; Supplementary Table S5). The peak features and proportions of these DARs in the genome were similar across each cell type, with most located in the distal intergenic region and intronic regions and a small fraction in the promoter and exon regions (Fig. 6B). These data indicated that all central corneal epithelial cell types undergo similar patterns of changes in chromatin accessibility in the early stages of wound healing.

To deepen our understanding of the physiologic function of these potential early wound-responsive elements, we

Investigative Ophthalmology & Visual Science

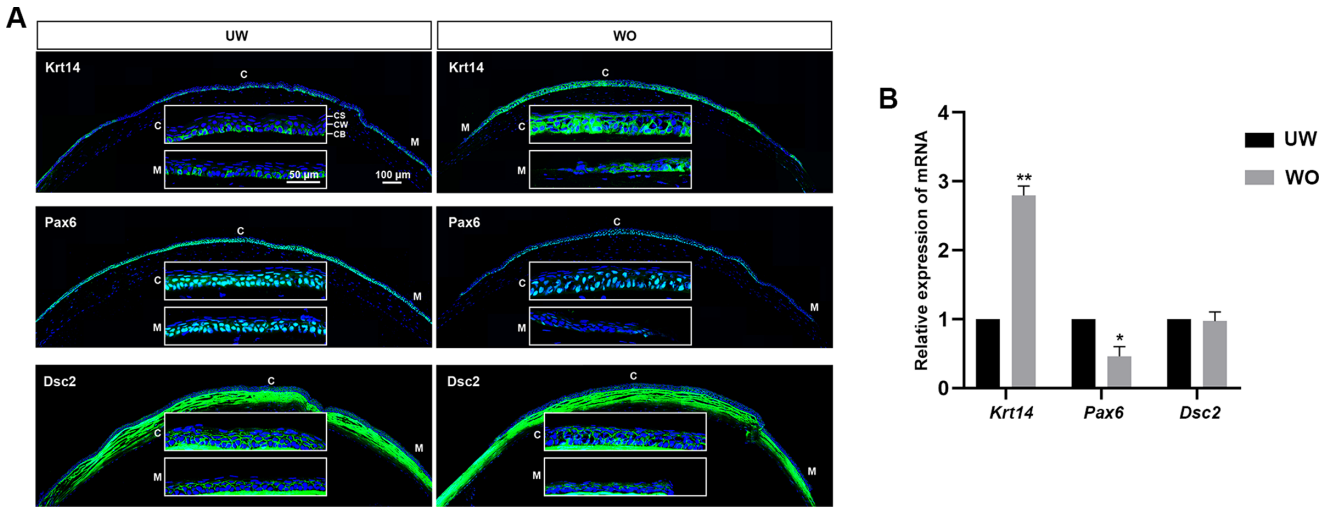

Figure 3. Validation of the wound-induced gene expression changes in mouse cornea. (**A**) Corneal cryosections from UW and WO mice were immunostained with the indicated antibodies. The *white rectangles* show the higher-magnification images of central and marginal areas of corneal epithelium. C, central area of corneal epithelium; M, marginal area of corneal epithelium. *Scale bars*: 100 μm for the whole cornea sections and 50 μm for the higher-magnification images. (**B**) Quantitative real-time PCR analysis of the indicated genes. Gapdh served as the endogenous control. *Error bars* represent SEM, $n = 3$. Statistical significance was assessed using multiple *t*-tests, $^{*}P < 0.05$, $^{**}P < 0.001$.

performed a more detailed subdivision of the DARs located in the distal intergenic region and promoter. Subsequently, we carried out bioinformatic analyses on their linked nearest genes. By counting the number of DARs in the corresponding intervals, we observed that most distal wound response elements were mainly located within 50 kb from the TSS, where enhancers are often identified (Fig. 6C). In the promoter regions, our results showed that there were more wound-responsive elements within 1 kb of the TSS (Fig. 6D). The nearest genes linked by distal DARs overlapped significantly among different cell types (Fig. 6E; Supplementary Fig. S8). Although the number of specific nearest genes linked by distal DARs located in the 0 to 50 bp of CS was the largest, it only accounted for 27.3% of their total linked genes. However, promoter DAR-linked nearest genes had relatively high specificity in all cell types, and the specific genes accounted for about 53.5% to 80.2% of their total genes (Fig. 6F; Supplementary Fig. S8). This suggests that distal regulatory elements may play a major role in regulating the common wound responses of different cell types in early wound healing. GO analysis of the shared nearest genes linked by distal DARs or promoter DARs revealed that the biological processes they regulated were all consistent with the biology of wound healing, including voltage-gated potassium channel activity, chemotaxis, peptidase activity, and cell motility (Figs. 6E, 6F; Supplementary Fig. S9). Altogether, these results provide insight into the corneal epithelial cells' chromatin accessibility landscape in the early response to wounds.

Fosl1/AP-1 TF-Binding Motif Is Enriched in Early Wound-Responsive Elements

To identify TFs that may be involved in chromatin remodeling and regulate the expression of genes during early wound response, we performed motif enrichment analysis to identify TF-binding sites in the differentially accessible regions. First, we analyzed all upregulated accessibility regions with ArchR. Our results showed that under normal homeostasis, the DNA motifs that were highly enriched in different cell types within the corneal epithelium were consistent with their specific cellular identities. For example, CBs were enriched in motifs for *Trp63*, which was associated with proliferation (Fig. 7A). For CWs and CSs, DNA motifs for epithelial differentiation, such as *Grhl1*, *Klf4*, and *Elf3*, were prominent (Figs. 7B, 7C). This observation is also in line with our previous report on cell type–specific transcriptional regulators in mouse corneal epithelium.[34] However, we observed very similar motifs across different cell types in the wounded corneas. Among them, AP-1 family binding motifs were relatively highly enriched sequences (Figs. 7D–F).

After that, we classified the wound-induced upregulated DARs and performed motif enrichment analysis again using HOMER software. We categorized these DARs in the distal intergenic and promoter regions into multiple intervals based on their distance from the TSS. Then, within each interval, we classified the DRAs into cell type–specific and cell type–shared groups based on the overlap of the nearest genes. By subdividing DARs in this way, we intended to identify a wider range of DNA motifs. Surprisingly, our results showed that almost all of the accessibility regions were highly enriched with the Fosl1/AP-1 TF binding site (Fig. 7G). We validated this result with the TF footprint analysis, as this method has been shown to correlate with TF binding (Supplementary Fig. S10).[44] At the same time, we also found the regulator activity of Fosl1 was increased in all corneal epithelial cell types after wounding by using pySCENIC in our scRNA-seq data (Supplementary Fig. S11).

Further, we performed IF staining and quantitative real-time PCR to investigate Fosl1 expression in UW and WO mouse corneas (Fig. 7H; Supplementary Fig. S4D). Consistent with our scATAC-seq and scRNA-seq data, we observed increased nuclear expression of Fosl1 in corneal epithelial cells of wounded mice compared with unwounded mice. The AP-1 transcriptional factors have been reported to regulate

Investigative Ophthalmology & Visual Science

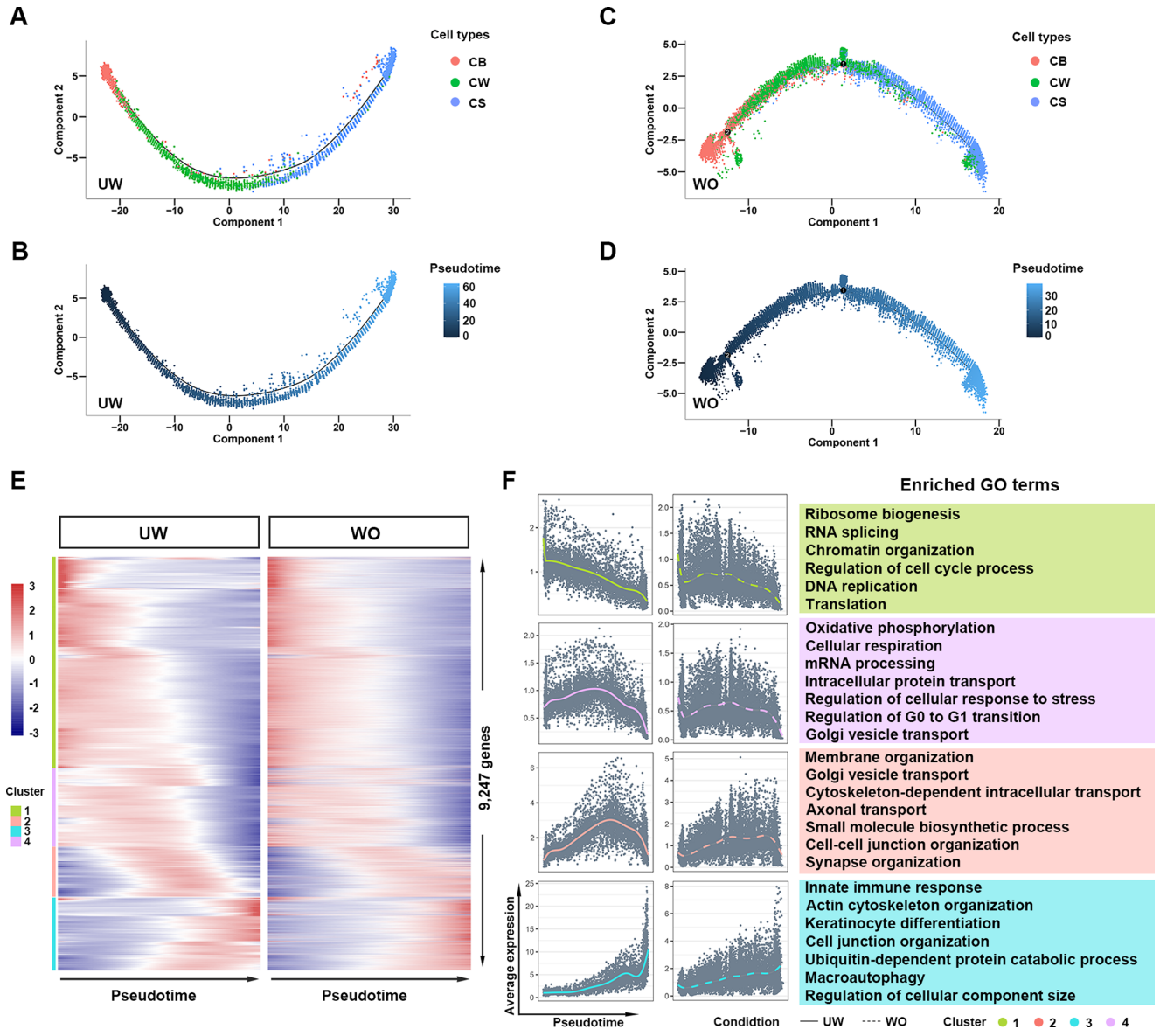

Figure 4. Pseudo-time trajectory analysis of corneal epithelial cells in UW and WO. The differentiation of UW (**A**, **B**) and WO (**C**, **D**) corneal epithelial cells along the pseudo-time trajectory. Color key from *dark* to *bright* indicates the differentiation process from the early to late stages. Each cell-type annotation is labeled to the *right*. (**E**) Heatmap showing the 9247 overlapped genes along the differentiation trajectory. Color key from *blue* to *red* indicates relative expression levels from low to high. (**F**) Average expression patterns (*left*) and enriched biological processes (*right*) of the four gene clusters along pseudo-time in (**E**). *Solid* and *dashed lines* indicate the average expression of a particular gene cluster in UW and WO samples, respectively. The enriched GO terms in each gene cluster are listed.

chromatin accessibility, but their specific regulatory mechanisms in cornea are still unclear.[45,46] Our results implied that Fosl1 may contribute to chromatin opening in a pan-binding manner during early corneal wound healing.

Changes in Chromatin Accessibility Are Less Concordant With Transcriptional Changes in Early Wound Response

Analysis of the relationship between changes in chromatin accessibility and changes in gene transcriptional activity is one of major approaches to understand various transcriptional regulatory programs.[47] To uncover the potential gene regulatory mechanisms underlying corneal epithelium in early wound healing, we analyzed the correlation of peak accessibility and gene expression in each cell type. A total of 22,303, 24,993, and 24,831 unique peak-to-gene links were identified in CBs, CWs, and CSs, respectively, with a similar proportion of peak features in each cell type (Figs. 8A, 8B; Supplementary Table S6). Unexpectedly, we found that the number of peak-to-gene links induced by wounds was significantly less than that of unwounded cornea, with only 6155, 5559, and 7659 in CBs, CWs, and CSs, respectively. This indicates that although a large number of changes in chromatin accessibility and gene expression were induced during early wound healing, their correlation was low.

Through GO enrichment analysis of the genes contained in these highly correlated links, we observed that although

Investigative Ophthalmology & Visual Science

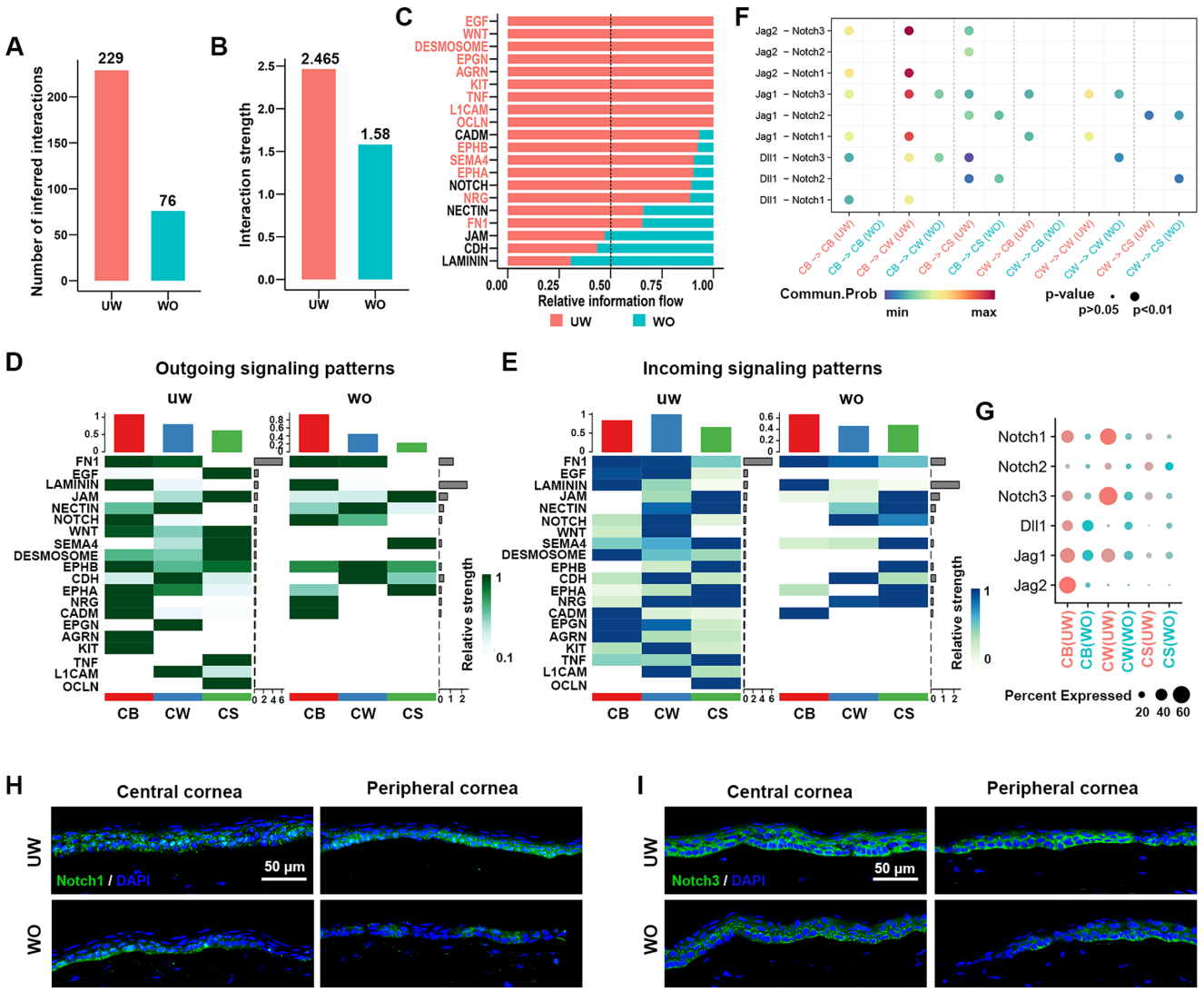

Figure 5. Cell–cell interactions in the UW and WO cornea. (**A**, **B**) Number and strength of inferred cellular interactions in the UW and WO cornea. (**C**) Bar charts showing the proportions of signaling pathways based on differences in overall information flow within inferred cellular interactions in UW and WO cornea. The color-coded pathways (*red*, *black*) denote their enrichment status in each group. (**D**, **E**) Outgoing or incoming signaling patterns in UW and WO cornea. (**F**) Comparison of the Notch pathway ligand–receptor pairs between the UW and WO cornea. (**G**) Dot plots displaying expression level of genes in the Notch pathway. (**H**, **I**) Corneal cryosections from UW and WO mice were immunostained with anti-Notch1 and anti-Notch3 antibodies. *Scale bars*: 50 μm.

gene regulation interactions of early wound healing differ in different epithelial cell types, they were mainly related to the biologic processes of wound repair, such as the apoptotic signaling pathway, peptidase activity, epithelial cell differentiation, and innate immune response (Fig. 8C). As for the unwounded cornea, these potential gene regulatory interactions are mainly related to the identity of their respective cell types, which is also in line with our previous study of mouse corneal cell type–specific gene regulatory programs (Fig. 8C).

Discussion

Injury is an inevitable part of every organism's life. Consequently, organisms have evolved rapid and efficient wound-healing mechanisms to repair damaged tissues. In this study, we described the transcriptome and chromatin accessibility changes of different corneal epithelial cell types in the early response to mechanical injury, aiming to enhance our understanding of the molecular mechanisms of wound healing.

We observed that corneal epithelium trauma resulted in dramatic transcriptomic and epigenetic alterations in the early stages of wound healing. Notably, the wound-induced genes and open chromatin regions are largely identical across different epithelial cell types, suggesting that epithelial cells share common wound response mechanisms during early wound repair, such as epithelial cell differentiation, apoptotic signaling pathway, and chromatin remodeling. Coincidentally, our findings are consistent with previous single-cell transcriptomic studies of axonal injury, musculoskeletal injury, and acute kidney injury in human and animal models, which have also shown similar injury-induced responses in different cell types during early wound repair.[41,48–50] Based on these similarities, we conjecture that early wound-induced responses may be widespread

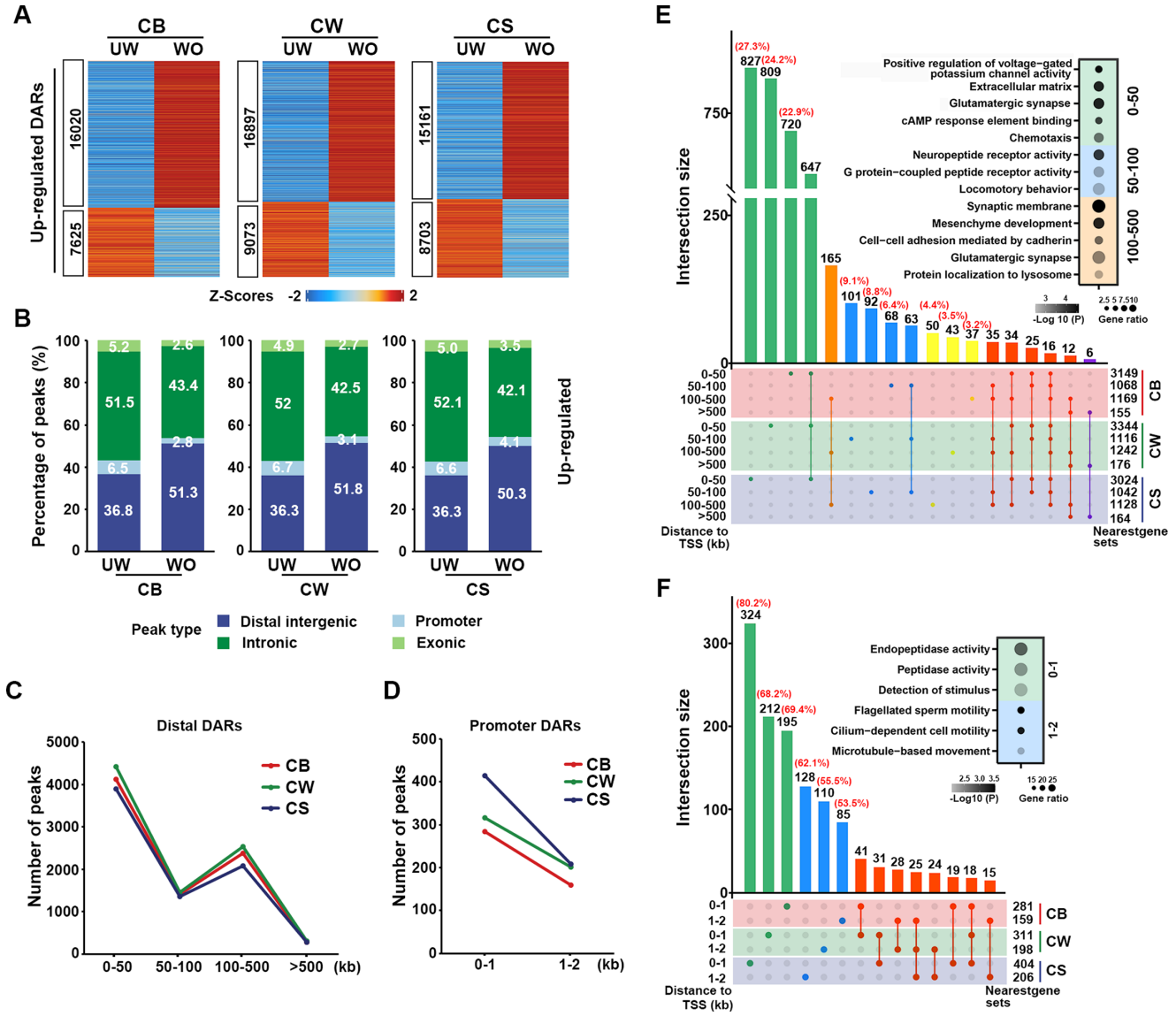

Figure 6. Early wound-induced chromatin accessibility changes in corneal epithelium. (**A**) Heatmaps of *z*-scores of upregulated DARs in CBs, CWs, and CSs from UW and WO corneas. (**B**) Bar graphs showing the percentage of marker peaks that mapped to exon, intron, promoter, or distal intergenic regions. (**C**, **D**) Line graphs showing the number of marker peaks within the indicated distal intergenic regions (**C**) and promoter regions (**D**) in CBs, CWs, and CSs. (**E**, **F**) Upset plot showing the size of overlaps among the sets of distal DARs (**E**) or promoter DARs (**F**) linked to the nearest genes identified in each cell type. The set size of the nearest genes linked by DARs within the indicated regions in each cell type is shown on the *left*. The bar plot at the *top* shows the number of overlapping genes between different sets or the number and percentage of unique genes in one set. GO terms for the overlapped gene sets within the indicated genome regions in three cell types, respectively.

at the wound site and are independent of the type of tissue cells and the mode of injury. However, we believe that more studies with different perspectives (e.g., different tissue, modes of injury) are still needed to test this conjecture.

Although transcriptional regulation through distal *cis*-elements is known to play pivotal roles in tissue development, differentiation, and disease, its role in corneal epithelial wound healing is unclear.[51,52] In this study, our data show for the first time that all corneal epithelial cell types undergo similar changes in chromatin accessibility during early wound healing and that these wound-induced open chromatins are mainly located in the distal intergenic region, suggesting that distal regulation is involved in the early wound-responsive program of corneal epithelial cells. Future studies need to further elucidate how changes in distal *cis*-elements affect the wound-healing process.

Changes in chromatin structure can affect the binding of TF to transcriptional regulatory elements, making it a well-known regulator of gene transcription.[53] We found that a significant number of wound-induced open chromatin regions were enriched with the Fosl1/AP-1 binding motif, suggesting that AP-1 TFs may play an essential role in the corneal epithelium response to injury. The transcription of AP-1 TFs has been shown to be rapidly activated by a variety of physiologic stimuli and environmental insults, but their physiologic functions are still being

Investigative Ophthalmology & Visual Science

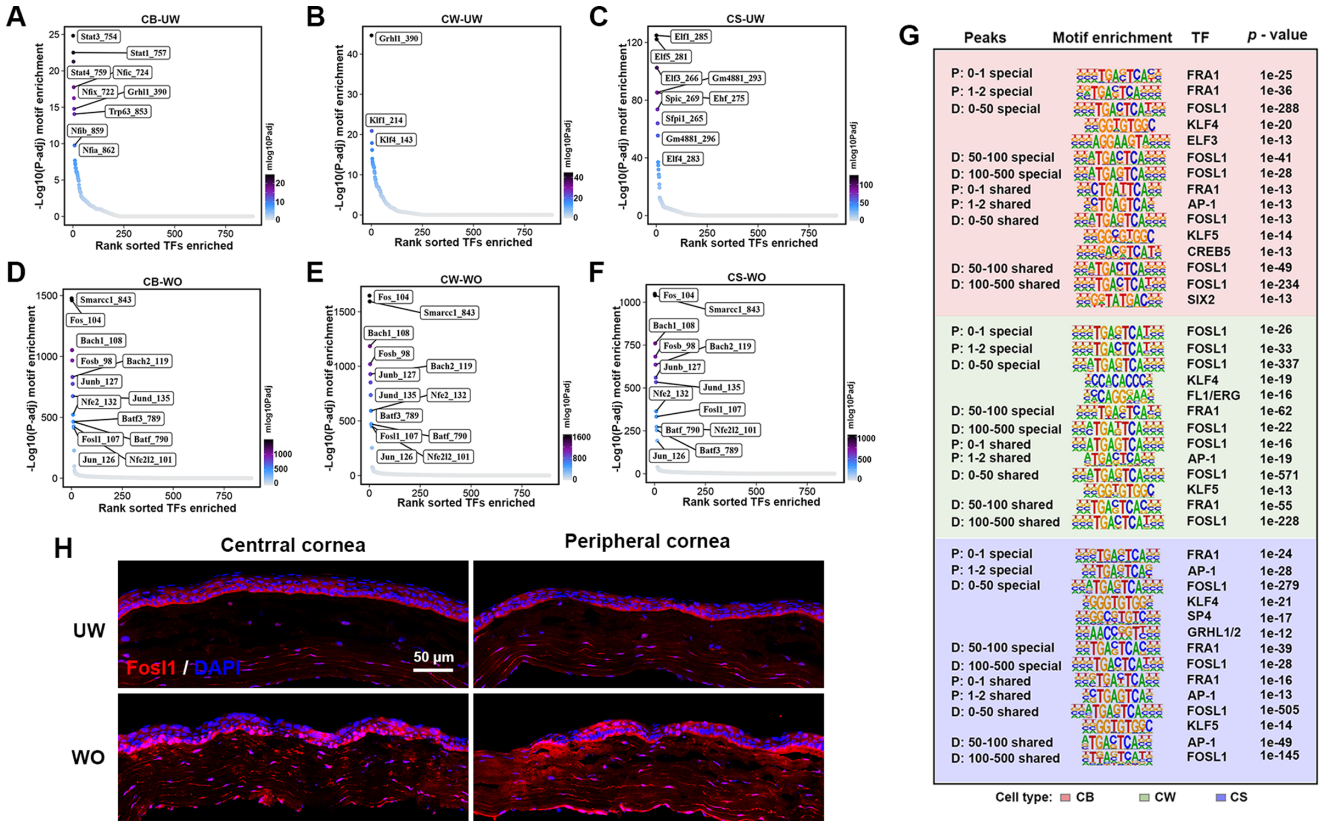

Figure 7. Motif enrichment analysis of DARs identified in the UW and WO mouse corneas. (**A–F**) Motif enrichment analysis using ArchR was performed on all upregulated DARs in three cell types from UW and WO corneas, respectively. (**G**) The motif and statistics from HOMER for the wound-induced upregulated DARs in the indicated regions of each cell type are provided. P: DARs located in the promoter region; D: DARs located in the distal intergenic region. (**H**) Corneal cryosections from UW and WO mice were immunostained with anti-Fosl1 antibody. *Scale bars*: 50 µm.

explored. Initially, AP-1 TFs were reported to regulate cellular processes such as cell proliferation, death, survival, differentiation, and migration.[54,55] Later, with the development of various sequencing technologies, more and more studies have shown that AP-1 can also be involved in regulating chromatin remodeling. For example, a study using the ATAC-seq technique showed that AP-1 TFs play an essential role in the injury responses of cardiomyocytes by regulating chromatin accessibility.[46] In the human umbilical vein endothelial cell line, Zhang et al.[56] identified that AP-1 TFs were capable of driving chromatin accessibility reconstruction and regulating senescence. Given that our results show that the Fosl1/AP-1 motif is significantly enriched and present in almost all open regions, this suggests that Fosl1 may be also a mediator of chromatin accessibility in the corneal epithelium. However, the relationship between changes in chromatin accessibility and corneal pathologic healing diseases, such as diabetic keratopathy, is unclear, and whether Fosl1 has an effect on it deserves further investigation.

As high-throughput sequencing-based methods have been used to investigate the relationship between chromatin accessibility and the resultant changes in transcription, there is considerable evidence that changes in chromatin accessibility can affect the binding of TF to transcriptional regulatory elements and thus regulate gene transcription.[57–59] However, multiple studies have also reported that changes in chromatin accessibility are not always concordant with changes in gene expression in some cases.[60–62] For instance, although stimulation of MCF-7 breast carcinoma cells with retinoic acid or TGF-β caused significant changes in transcriptome and chromatin accessibility, many of these gene expression changes occurred independently of changes in the accessibility of local chromatin.[47] These observations imply that the relationship between chromatin accessibility and gene expression is complex and probably context dependent. Here, we found that while there was a high degree of concordance between some wound-induced gene expression and changes in chromatin accessibility, most genes were less correlated with chromatin accessibility in wounded corneas compared to unwounded corneas. Based on previous similar reports, we reason that changes in chromatin accessibility in the early stages of corneal epithelium wound healing not only ensure the activation of specific genes but may also reflect the consequences of exposure to certain extracellular stimuli or provide a platform upon which TFs can regulate some gene transcription.

Limitations of the Study

There are some limitations to the current data set, which may affect a full understanding of the molecular mechanisms of corneal wound healing. The analysis is limited to a single time point (3 hours after wounding), which may not capture the full temporal dynam-

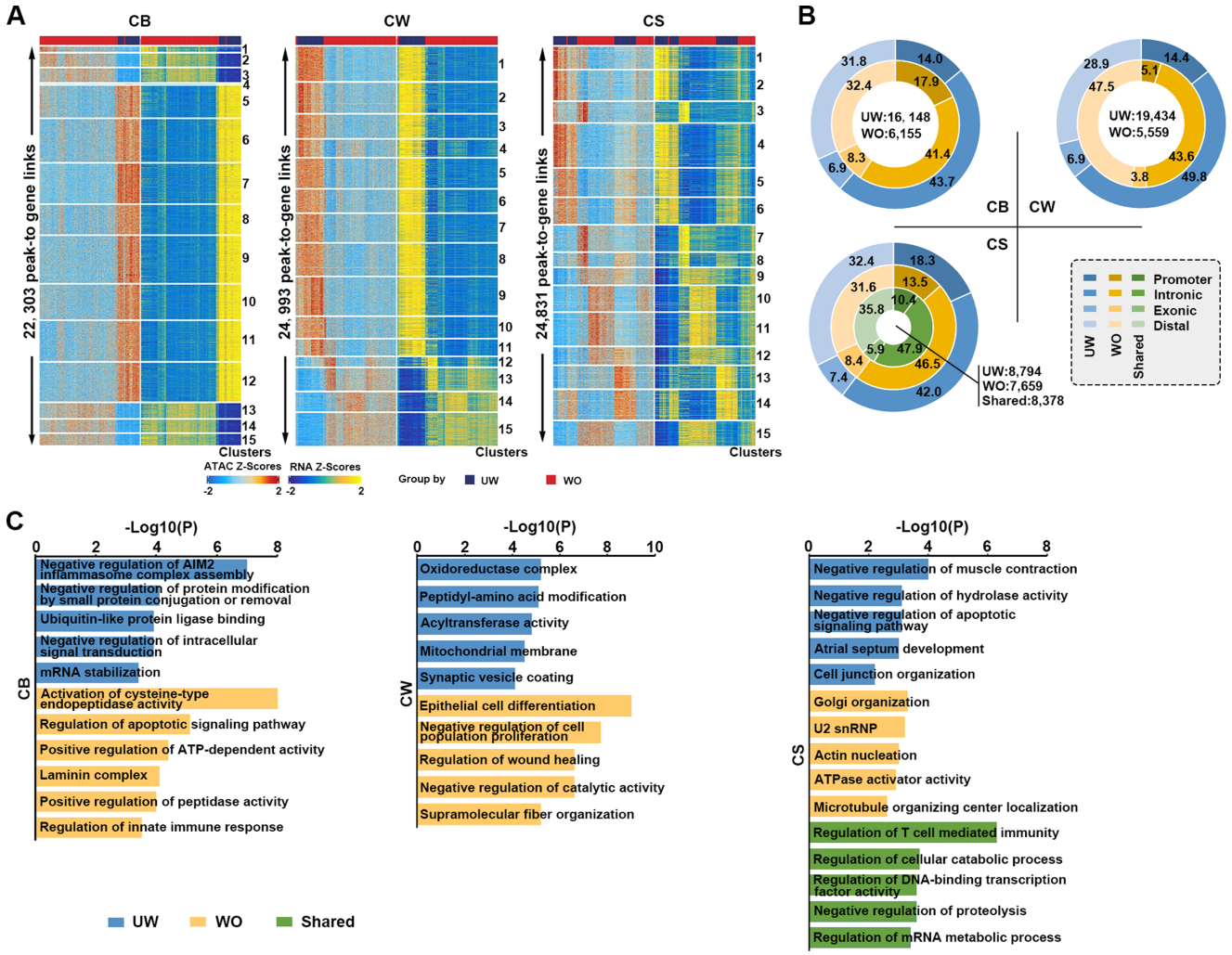

Figure 8. Analysis of the concordance between changes in gene expression and changes in chromatin accessibility. (**A**) Heatmaps showing the column *z*-score of normalized accessibility and integrated gene expression of peak-to-gene links from the UW and WO corneas in each cell type. Each row represents a pair of one CRE and one linked gene. Each CRE can be linked to multiple genes, and each gene can be linked to multiple CREs. Pairs (rows) were clustered into 15 clusters. (**B**) Donut plots showing the distribution patterns of DARs in each cell type. UW: DARs from the peak-to-gene links that only present in the UW cornea; WO: DARs from the peak-to-gene links that only present in the WO cornea; Shared: DARs from the peak-to-gene links that present in both the UW and WO cornea. (**C**) GO term enrichment of the indicated peak-linked genes in each cell type. UW: peak-to-gene links that only present in the UW cornea; WO: peak-to-gene links that only present in the WO cornea; Shared: peak-to-gene links that present in both the UW and WO cornea.

ics of the wound-healing process. Future studies will integrate multiomics analyses across sequential time points to capture the full temporal dynamics of wound healing and provide a more comprehensive understanding of the process. In addition, although our findings suggest that Fosl1/AP-1 contributes to chromatin remodeling during corneal wound healing, this remains speculative without direct experimental validation. Future studies will employ lineage-specific Fosl1 knockout models to confirm its role.

Conclusions

In conclusion, our study delineates the gene expression and chromatin accessibility changes in different mouse corneal epithelial cell types and enhances our understanding of early wound response programs. Our findings may provide insights into therapeutic options for studying corneal pathologic healing. Meanwhile, our data set could serve as a resource for further research on the molecular mechanisms of wound healing.

Acknowledgments

The authors thank the staff of the Laboratory Animal Center and the staff of the Core Facilities at State Key Laboratory of Ophthalmology, Zhongshan Ophthalmic Center for technical support.

Supported by CAMS Innovation Fund for Medical Sciences (2019-I2M-5-005), State Key Laboratory of Ophthalmology, Zhongshan Ophthalmic Center, Sun Yat-Sen University, Guangdong Provincial Key Laboratory of Ophthalmology and Visual Science, Guangzhou, China. The funding body had no role in study design, collection, management, analysis and interpretation of data, writing of the manuscript, and the decision to submit the manuscript for publication.

Disclosure: **Z.-J. Lu**, None; **J.-G. Ye**, None; **J.-N. Li**, None; **J.-B. Liang**, None; **M. Zhou**, None; **Q.-L. Hu**, None; **Q.-K. Zhang**, None; **Y.-H. Lin**, None; **Y.-F. Zheng**, None

References

1. Cordeiro JV, Jacinto A. The role of transcription-independent damage signals in the initiation of epithelial wound healing. *Nat Rev Mol Cell Biol*. 2013;14:249–262.
2. Dekoninck S, Blanpain C. Stem cell dynamics, migration and plasticity during wound healing. *Nat Cell Biol*. 2019;21:18–24.
3. Zhou SX, Xie MB, Su JJ, Cai BJ, Li JA, Zhang K. New insights into balancing wound healing and scarless skin repair. *J Tissue Eng*. 2023;14:20417314231185848.
4. Nirenjen S, Narayanan J, Tamilanban T, et al. Exploring the contribution of pro-inflammatory cytokines to impaired wound healing in diabetes. *Front Immunol*. 2023;14:1216321.
5. Nikoloudaki G, Brooks S, Peidl AP, Tinney D, Hamilton DW. JNK signaling as a key modulator of soft connective tissue physiology, pathology, and healing. *Int J Mol Sci*. 2020;21:1015.
6. Xiao WR, Tang H, Wu M, et al. Ozone oil promotes wound healing by increasing the migration of fibroblasts via PI3K/Akt/mTOR signaling pathway. *Bioscience Rep*. 2017;37:BSR20170658.
7. He J, Qi D, Wang DX, et al. Insulin upregulates the expression of epithelial sodium channel in vitro and in a mouse model of acute lung injury: role of mTORC2/SGK1 pathway. *Exp Cell Res*. 2015;331:164–175.
8. Warren R, Lyu HD, Klinkhammer K, De Langhe SP. Hippo signaling impairs alveolar epithelial regeneration in pulmonary fibrosis. *Elife*. 2023;12:e85092.
9. Liu Y, Xu CH, Li JH, et al. YAP promotes AP-1 expression in tubular epithelial cells in the kidney. *Am J Physiol Renal*. 2023;324:F581–F589.
10. Kakanj P, Moussian B, Gronke S, et al. Insulin and TOR signal in parallel through FOXO and S6K to promote epithelial wound healing. *Nat Commun*. 2016;7:12972.
11. Migdal M, Tralle E, Abu Nahia K, et al. Multi-omics analyses of early liver injury reveals cell-type-specific transcriptional and epigenomic shift. *BMC Genomics*. 2021;22:904.
12. Kirita Y, Wu HJ, Uchimura K, Wilson PC, Humphreys BD. Cell profiling of mouse acute kidney injury reveals conserved cellular responses to injury. *Proc Natl Acad Sci USA*. 2020;117:15874–15883.
13. Vizcaya-Molina E, Klein CC, Serras F, Mishra RK, Guigó R, Corominas M. Damage-responsive elements in regeneration. *Genome Res*. 2018;28:1852–1866.
14. Stepp MA, Zieske JD, Trinkaus-Randall V, et al. Wounding the cornea to learn how it heals. *Exp Eye Res*. 2014;121:178–193.
15. Chang CY, Green CR, McGhee CNJ, Sherwin T. Acute wound healing in the human central corneal epithelium appears to be independent of limbal stem cell influence. *Invest Ophthalmol Vis Sci*. 2008;49:5279–5286.
16. Puri S, Sun MX, Mutoji KN, Gesteira TF, Coulson-Thomas VJ. Epithelial cell migration and proliferation patterns during initial wound closure in normal mice and an experimental model of limbal stem cell deficiency. *Invest Ophthalmol Vis Sci*. 2020;61:27.
17. Nasser W, Amitai-Lange A, Soteriou D, et al. Corneal-committed cells restore the stem cell pool and tissue boundary following injury. *Cell Rep*. 2018;22:323–331.
18. Ljubimov AV, Saghizadeh M. Progress in corneal wound healing. *Prog Retin Eye Res*. 2015;49:17–45.
19. Kalha S, Kuony A, Michon F. Corneal epithelial abrasion with ocular burr as a model for cornea wound healing. *J Vis Exp*. 2018;10:58071.
20. Altshuler A, Amitai-Lange A, Tarazi N, et al. Discrete limbal epithelial stem cell populations mediate corneal homeostasis and wound healing. *Cell Stem Cell*. 2021;28:1248–1261.e1248.
21. Kaplan N, Wang J, Wray B, et al. Single-cell RNA transcriptome helps define the limbal/corneal epithelial stem/early transit amplifying cells and how autophagy affects this population. *Invest Ophthalmol Vis Sci*. 2019;60:3570–3583.
22. Shi W, Ye J, Shi Z, et al. Chromatin accessibility analysis reveals regulatory dynamics and therapeutic relevance of Vogt-Koyanagi-Harada disease. *Commun Biol*. 2022;5:506.
23. Stuart T, Butler A, Hoffman P, et al. Comprehensive integration of single-cell data. *Cell*. 2019;177:1888–1902.e1821.
24. Korsunsky I, Millard N, Fan J, et al. Fast, sensitive and accurate integration of single-cell data with Harmony. *Nat Methods*. 2019;16:1289–1296.
25. Pont F, Tosolini M, Fournie JJ. Single-cell signature explorer for comprehensive visualization of single cell signatures across scRNA-seq datasets. *Nucleic Acids Res*. 2019;47:e133.
26. Lupasco T, He ZG, Cassagne M, et al. Corneal epithelium in keratoconus underexpresses active NRF2 and a subset of oxidative stress-related genes. *Plos One*. 2022;17:e0273807.
27. Qiu X, Mao Q, Tang Y, et al. Reversed graph embedding resolves complex single-cell trajectories. *Nat Methods*. 2017;14:979–982.
28. Jin S, Plikus MV, Nie Q. CellChat for systematic analysis of cell-cell communication from single-cell transcriptomics. *Nat Protoc*. 2025;20:180–219.
29. Granja JM, Corces MR, Pierce SE, et al. ArchR is a scalable software package for integrative single-cell chromatin accessibility analysis. *Nat Genet*. 2021;53:403–411.
30. van Dijk D, Sharma R, Nainys J, et al. Recovering gene interactions from single-cell data using data diffusion. *Cell*. 2018;174:716–729.e727.
31. Heinz S, Benner C, Spann N, et al. Simple combinations of lineage-determining transcription factors prime cis-regulatory elements required for macrophage and B cell identities. *Mol Cell*. 2010;38:576–589.
32. Aibar S, Gonzalez-Blas CB, Moerman T, et al. SCENIC: single-cell regulatory network inference and clustering. *Nat Methods*. 2017;14:1083–1086.
33. Zhou Y, Zhou B, Pache L, et al. Metascape provides a biologist-oriented resource for the analysis of systems-level datasets. *Nat Commun*. 2019;10:1523.
34. Lu ZJ, Ye JG, Wang DL, et al. Integrative single-cell RNA-seq and ATAC-seq analysis of mouse corneal epithelial cells. *Invest Ophthalmol Vis Sci*. 2023;64:30.
35. Pajooresh-Ganji A, Pal-Ghosh S, Simmens SJ, Stepp MA. Integrins in slow-cycling corneal epithelial cells at the limbus in the mouse. *Stem Cells*. 2006;24:1075–1086.
36. Laux-Fenton WT, Donaldson PJ, Kistler J, Green CR. Connexin expression patterns in the rat cornea—molecular evidence for communication compartments. *Cornea*. 2003;22:457–464.
37. Yu FX, Gipson IK, Guo Y. Differential gene expression in healing rat corneal epithelium. *Invest Ophthalmol Vis Sci*. 1995;36:1997–2007.
38. Steiner CA, Cartwright IM, Taylor CT, Colgan SP. Hypoxia-inducible factor as a bridge between healthy barrier function, wound healing, and fibrosis. *Am J Physiol Cell Physiol*. 2022;323:C866–C878.
39. Harding HP, Zhang Y, Zeng H, et al. An integrated stress response regulates amino acid metabolism and resistance to oxidative stress. *Mol Cell*. 2003;11:619–633.

Investigative Ophthalmology & Visual Science

40. Thomasova D, Mulay SR, Bruns H, Anders HJ. p53-independent roles of MDM2 in NF-kappaB signaling: implications for cancer therapy, wound healing, and autoimmune diseases. *Neoplasia*. 2012;14:1097–1101.
41. Renthal W, Tochitsky I, Yang L, et al. Transcriptional reprogramming of distinct peripheral sensory neuron subtypes after axonal injury. *Neuron*. 2020;108:128–144.e129.
42. Movahedan A, Majdi M, Afsharkhamseh N, et al. Notch inhibition during corneal epithelial wound healing promotes migration. *Invest Ophthalmol Vis Sci*. 2012;53:7476–7483.
43. Djalilian AR, Namavari A, Ito A, et al. Down-regulation of Notch signaling during corneal epithelial proliferation. *Mol Vis*. 2008;14:1041–1049.
44. Youn A, Marquez EJ, Lawlor N, Stitzel ML, Ucar D. BiFET: sequencing Bias-free transcription factor Footprint Enrichment Test. *Nucleic Acids Res*. 2019;47:e11.
45. Yukawa M, Jagannathan S, Vallabh S, et al. AP-1 activity induced by co-stimulation is required for chromatin opening during T cell activation. *J Exp Med*. 2020;217:e20182009.
46. Beisaw A, Kuenne C, Guenther S, et al. AP-1 contributes to chromatin accessibility to promote sarcomere disassembly and cardiomyocyte protrusion during zebrafish heart regeneration. *Circ Res*. 2020;126:1760–1778.
47. Kiani K, Sanford EM, Goyal Y, Raj A. Changes in chromatin accessibility are not concordant with transcriptional changes for single-factor perturbations. *Mol Syst Biol*. 2022;18:e10979.
48. Kirita Y, Wu H, Uchimura K, Wilson PC, Humphreys BD. Cell profiling of mouse acute kidney injury reveals conserved cellular responses to injury. *Proc Natl Acad Sci USA*. 2020;117:15874–15883.
49. Hinze C, Kocks C, Leiz J, et al. Single-cell transcriptomics reveals common epithelial response patterns in human acute kidney injury. *Genome Med*. 2022;14:103.
50. Tower RJ, Bancroft AC, Chowdary AR, et al. Single-cell mapping of regenerative and fibrotic healing responses after musculoskeletal injury. *Stem Cell Rep*. 2022;17:2334–2348.
51. Schoenfelder S, Fraser P. Long-range enhancer-promoter contacts in gene expression control. *Nat Rev Genet*. 2019;20:437–455.
52. Riethoven JJ. Regulatory regions in DNA: promoters, enhancers, silencers, and insulators. *Methods Mol Biol*. 2010;674:33–42.
53. Misteli T, Finn EH. Chromatin architecture is a flexible foundation for gene expression. *Nat Genet*. 2021;53:426–427.
54. Shaulian E, Karin M. AP-1 as a regulator of cell life and death. *Nat Cell Biol*. 2002;4:E131–E136.
55. Shaulian E, Karin M. AP-1 in cell proliferation and survival. *Oncogene*. 2001;20:2390–2400.
56. Zhang C, Zhang X, Huang L, et al. ATF3 drives senescence by reconstructing accessible chromatin profiles. *Aging Cell*. 2021;20:e13315.
57. Wang Z, Cui M, Shah AM, et al. Cell-type-specific gene regulatory networks underlying murine neonatal heart regeneration at single-cell resolution. *Cell Rep*. 2021;35:109211.
58. Becker WR, Nevins SA, Chen DC, et al. Single-cell analyses define a continuum of cell state and composition changes in the malignant transformation of polyps to colorectal cancer. *Nat Genet*. 2022;54:985–995.
59. Diedrich JD, Dong Q, Ferguson DC, et al. Profiling chromatin accessibility in pediatric acute lymphoblastic leukemia identifies subtype-specific chromatin landscapes and gene regulatory networks. *Leukemia*. 2021;35:3078–3091.
60. Chen D, Parker TM, Bhat-Nakshatri P, et al. Nonlinear relationship between chromatin accessibility and estradiol-regulated gene expression. *Oncogene*. 2021;40:1332–1346.
61. Yu D, Zhang T, Zhou G, et al. Co-profiling reveals distinct patterns of genomic chromatin accessibility and gene expression in pulmonary hypertension caused by chronic hypoxia. *Respir Res*. 2023;24:104.
62. Perrin HJ, Currin KW, Vadlamudi S, et al. Chromatin accessibility and gene expression during adipocyte differentiation identify context-dependent effects at cardiometabolic GWAS loci. *PLoS Genet*. 2021;17:e1009865.

Investigative Ophthalmology & Visual Science